Inorganic Chemistry

Article

pubs.acs.org/IC

Flux Crystal Growth and Optical Properties of Two Uranium-Containing Silicates: A_2USiO_6 (A = Cs, Rb)

Cory Michael Read,[†] Mark D. Smith,[†] Ray Withers,[‡] and Hans-Conrad zur Loye*[,†]

[†]Department of Chemistry and Biochemistry, University of South Carolina, Columbia, South Carolina 29208, United States

[‡]Research School of Chemistry, The Australian National University, Canberra, Australian Capital Territory 0200, Australia

Supporting Information

ABSTRACT: Single crystals of two uranium silicates, Cs_2USiO_6 and Rb_2USiO_6, have been grown from molten fluoride fluxes and structurally characterized by single-crystal X-ray diffraction. Cs_2USiO_6 crystallizes in the body-centered orthorhombic space group, *Immm*, with a = 8.5812(4) Å, b = 13.0011(6) Å, and c = 13.8811(7) Å. The size of Rb is slightly too small to fit into this structural framework without effecting slight structural changes that result in a 6-fold superstructure. Sharp satellite peaks were observed in the single-crystal X-ray diffraction data, indicating the existing of a superstructure. The crystals were examined by electron diffraction, the results of which suggest that the structure can be thought of as the *Immm* isotype (a = 8.4916(6) Å, b = 12.6678(9) Å, and c = 13.5077(9) Å) on average, with an approximately 6-fold superstructure along the c axis. The materials were further characterized by UV−vis reflectance spectroscopy.

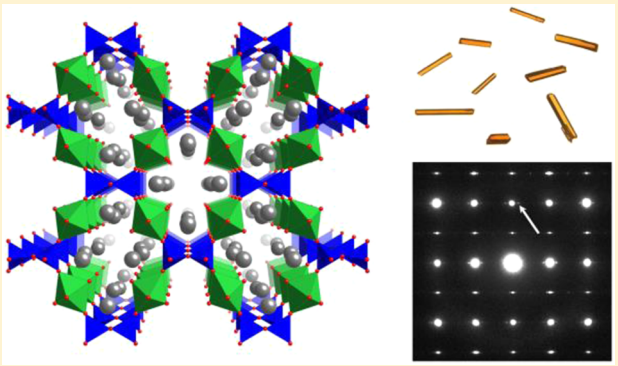

INTRODUCTION

There continues to be a growing concern of how to properly dispose of long-term nuclear waste. To date, geological repositories have been the most widely proposed method for long-term storage, and identifying the best structure types in which to confine radioisotopes to ensure long-term stability is a work in progress. Current immobilization procedures include the use of hydraulic cements, bitumen, and vitreous waste forms that include borosilicate and phosphate glasses as well as, more recently, crystalline materials that include monazite, garnets, and apatites. Important parameters for evaluating waste forms include leaching rates and resistance toward radiation damage, leading to amorphization.[1] Since numerous uranium-containing silicate minerals have persisted in nature for geologic time scales, crystalline silicates are, thus, one class of materials that could potentially be used to confine uranium for long-term storage. A large number of uranium silicates have been reported during the past decade,[2−12] including several that contain reduced uranium, U^{4+} or U^{5+}, rather than U^{6+}, the most common oxidation state found among oxides.

Nearly all of the uranium silicates reported in the literature exhibit three-dimensional (3D), infinite framework structures composed of UO_6, UO_7, and/or UO_8 polyhedra and SiO_4 tetrahedra.[2−16] One exceptional 2D structure exists, where two uranophane topological sheets are connected via corner-sharing with UO_6 octahedra, creating 2D slabs that are separated by sodium cations within the structure.[8] All of the exclusively uranium(VI) silicates exhibit typical uranyl coordination, with two short and four or five long U−O bonds. With respect to just the uranium polyhedral connectivities in the 3D uranium silicates, structures exist with 0D, 1D, and 3D networks. The 3D uranium networks are formed exclusively in reduced uranium-containing silicates, and no cation−cation interactions (CCIs) were observed in hexavalent uranium silicates, as the uranyl oxygen atoms were terminal. The SiO_4 tetrahedra form as discrete units, dimers, rings, chains, and sheets, where the Si concentration in the final product correlates with an increase in the dimensionality of the silicate network. The uranium and silicate networks assemble in three dimensions predominantly by corner sharing of uranium- and silicon-based polyhedra.

The synthetic uranium silicate materials have been prepared by various methods, and property characterization has been performed on several of the compounds. For example, magnetic data for hydrothermally grown, reduced uranium-containing silicates shows antiferromagnetic ordering.[4,9] Several of the fully oxidized uranium silicates exhibit room-temperature luminescence that has been linked to the uranyl environment.[5,7,11,14] Crystal growth of uranium-containing silicates has been achieved by solid state processing,[14] hydrothermal growth,[2−4,6,8−13] and flux crystal growth.[5,7]

Herein, we present the crystal growth of two hexavalent uranium silicates, Cs_2USiO_6 and Rb_2USiO_6. The Cs compound presented no unusual crystallographic difficulties and was a routine solution and refinement. The Rb analog, however, exhibits a structure modulation that was observed in both the

Received: February 13, 2015
Published: April 16, 2015

DOI: 10.1021/acs.inorgchem.5b00364
Inorg. Chem. 2015, 54, 4520−4525

single-crystal X-ray diffraction and the electron diffraction data, and that is discussed in some detail herein.

EXPERIMENTAL DETAILS

Reagents. U_3O_8 (International Bioanalitics Industries Inc., ACS grade), SiO_2 (Aldrich, 99.99%), RbF (Alfa Aesar, 99.7%), and CsF (Strem, 99+%) were used as received.

Caution: U_3O_8 contains depleted uranium, but standard precautions for handling radioactive and highly toxic substances should be followed.

Synthesis. Single crystals of Cs_2USiO_6 and Rb_2USiO_6 were grown from molten fluoride fluxes. A 0.33 mmol amount of U_3O_8, 1 mmol of SiO_2, and 40 mmol of *A*F (*A* = Cs, Rb) were added to a silver crucible and covered with a silver lid. The charge was heated to 900 °C at a rate of 10 °C/min, allowed to dwell for 12 h, cooled to 700 °C at a rate of 0.1 °C/min, and finally cooled to room temperature by turning the furnace off. The excess flux was removed by dissolution in H_2O, assisted by sonication. Phase-pure products in approximately 90% yield, based on U, were easily obtained by sonicating in water for at least 3 h. On the basis of the synthesis conditions, the compositions should be stable to at least 700 °C.

Single-Crystal X-ray Diffraction. *Cs_2SiUO_6.* X-ray intensity data from orange needle crystals were collected at 296(2) K using a Bruker SMART APEX diffractometer (Mo Kα radiation, λ = 0.71073 Å).[17] The data collection covered 98.3% of reciprocal space to $2\theta_{max}$ = 65.1°, with an average reflection redundancy of 10.2 and R_{int} = 0.056 after absorption correction. The raw area detector data frames were reduced and corrected for absorption effects with the SAINT+ and SADABS programs.[17] Final unit cell parameters were determined by least-squares refinement of 2813 reflections from the data set. Initial direct methods structure solution using SHELXS[18] located all metal atoms. Subsequent difference Fourier calculations located the remaining oxygen atoms. Refinement of the structural model by full-matrix least-squares against F^2 was performed with SHELXL2013/2[18] using the ShelXLe interface.[19] The compound crystallizes in the orthorhombic system. The pattern of systematic absences in the intensity data was consistent with a body-centered lattice but not with the presence of glide plane symmetry. The space group *Immm* (No. 71) was eventually determined to be correct. There are 11 independent atomic positions in the asymmetric unit, distributed over eight crystallographically distinct positions. One unique uranium U(1) is located on a mirror plane (site 8*k*, *m*.. site symmetry): four cesium atoms Cs(1)−Cs(4) are located on sites with C_{2v} point symmetry (Cs(1) and Cs(2) on sites 4*i* and 4*j*, respectively, with *mm*2 site symmetry, and Cs(3) and Cs(4) on sites 4*h* and 4*g*, respectively, with *m*2*m* site symmetry), and one silicon atom is located on a mirror plane (site 8*m*, .*m*. site symmetry). There are five oxygen atoms: O(1) and O(2) are located on general positions (site 16*o*), O(3) is located on a mirror plane (site 8*l*, *m*.. site symmetry), O(4) is located on site 4*j* (*mm*2 symmetry), and O(5) is located on site 4*e* (2*mm* site symmetry). All atoms were refined with anisotropic displacement parameters. Trial refinements of the site occupancies of the metal atoms showed no deviation from full occupancy. The largest residual electron density peak and hole in the final difference map are +1.56 and −2.28 e/Å^3, located 0.71 and 0.96 Å from Cs(1) and O(4), respectively.

Rb_2USiO_6. Crystals of Rb_2USiO_6 are orange rectangular rods, visually excellent with sharp extinctions of polarized light. Diffraction pattern quality is high, with narrow peak shapes and strong intensities. Using strong reflections, the diffraction pattern can be indexed to an orthorhombic *I* lattice with $a \approx 8.49$ Å, $b \approx 12.67$ Å, $c \approx 13.51$ Å, and $V \approx 1453.0$ Å^3. These parameters indicate Rb_2USiO_6 is structurally analogous to Cs_2USiO_6. (*Immm*; $a \approx 8.58$ Å, $b \approx 13.00$ Å, $c \approx 13.88$ Å, and $V \approx 1548.6$ Å^3). Cs_2USiO_6 presented no unusual crystallographic difficulties and was a routine solution and refinement. In the case of Rb_2USiO_6, this small cell leaves many unindexed spots, suggesting either twinning or a larger unit cell. Attempts from several crystals to index the diffraction data to multiple twin domains failed. Careful inspection of the diffraction spots shows the weaker reflections have indices near 1/3 or multiples thereof. Reindexing the diffraction pattern accounting for the weaker reflections consistently gave a primitive orthorhombic lattice with $a \approx 8.49$ Å, $b \approx 12.67$ Å, $c \approx 81.0$ Å, and $V \approx 8716$ Å^3 from several crystals. This corresponds to a 6-fold superstructure with $a' = a$, $b' = b$, and $c' = 6c$. Many attempts to solve the 6-fold superstructure have all failed. The pattern of systematic absences is not consistent with an orthorhombic space group. Ab initio solution methods (direct, heavy atom, charge flipping) did not yield sensible solutions. Attempts using lowered symmetry, including reducing to space group *P*1 (No. 1), followed by various searching methods for higher symmetry were also unsuccessful. This strategy generally proceeded by assuming the U and Rb atomic positions in six *Immm* subcells expanded by translation symmetry along [001] would correspond to the U and Rb positions in the sextupled cell. After enlarging the unit cell by $c' = 6c$, the computed U and Rb atomic positions were input and this model refined. Si atom positions were readily located, followed by many oxygen atom positions. Some progress was made with this approach, but these solutions were all unsatisfactory because of high instability in atomic positions and displacement parameters and the high *R* values. Refinements in space groups *P*1, *P*-1, *Pmma*, and *Pnnm* gave similar statistics, reaching a minimum at ca. *R*1 = 10%. Therefore, as an approximation of the true modulated structure, the averaged substructure is presented here, refined in space group *Immm*, isostructural with Cs_2USiO_6. Solution and refinement in the *Immm* subcell converges at *R*1 (*F*) = 0.037, with acceptable anisotropic displacement parameters (ADPs) for the U, Rb, and Si atoms but with some large and elongated oxygen atom ellipsoids, especially prominent for two silicate oxygens. The two atoms with pronounced ADP elongation are O2 and O5, which, along with their symmetry equivalents, form the four opposite triangular faces of the Si_4O_{12} cluster. Silicate oxygen O4, which links the Si_4O_{12} cluster along the crystallographic [100] direction, has a normal ADP. For the final model, O2 and O5 were refined isotropically with equally occupied split positions (A/B). All other atomic positions are analogous to those in the Cs_2USiO_6 type. With this model the largest residual electron density peak and hole are +2.27 (0.78 Å from U1) and −2.99 e/Å (1.07 Å from O4). Atoms O2 and O5 and the largest U_{ij} components of their ADPs lie in the crystallographic (*bc*) plane of the *Immm* cell. This suggests a structural modulation generated by a twisting of the opposite parallel faces of the Si_4O_{12} group, also affecting the UO_6 octahedra. Crystallographic data for the title compounds can be found in Table 1.

Electron Diffraction. The electron diffraction data were collected on a JEOL 2100F Transmission Electron Microscope operating at 200 keV. Samples for examination were prepared using crushed single crystals dispersed onto holey carbon-coated copper grids.

Powder X-ray Diffraction. Powder X-ray diffraction data were collected on a Rigaku D/Max-2100 powder X-ray diffractometer using Cu Kα radiation. The step scan covered the angular range 5−70° 2θ in

Table 1. Crystallographic Data for Cs_2USiO_6 and the Analogous Average Structure of Rb_2USiO_6

empirical formula	Cs_2USiO_6	Rb_2USiO_6
fw (amu)	627.94	533.06
cryst syst	orthorhombic	orthorhombic
space group	*Immm*	*Immm*
a (Å)	8.5812(4)	8.4916(6)
b (Å)	13.0011(6)	12.6678(9)
c (Å)	13.8811(7)	13.5077(9)
vol. (Å^3)	1548.65(13)	1453.02(17)
Z	8	8
ρ_{calc} (g/mm^3)	5.386	4.874
μ (mm^{-1})	30.357	35.790
temp. (K)	296(2)	296(2)
wavelength (Å)	0.71073	0.71073
final *R* indexes [$I > 2\sigma(I)$]	R_1 = 0.0253, wR_2 = 0.0506	R_1 = 0.0369, wR_2 = 0.0918
final *R* indexes [all data]	R_1 = 0.0327, wR_2 = 0.0531	R_1 = 0.0457, wR_2 = 0.0965

DOI: 10.1021/acs.inorgchem.5b00364
Inorg. Chem. 2015, 54, 4520−4525

steps of 0.02°. No impurities were observed, and the calculated and experimental PXRD patterns are in excellent agreement (see Figures S1 and S2, Supporting Information).

Energy-Dispersive Spectroscopy (EDS). Elemental analysis was performed on the flux-grown crystals using a TESCAN Vega-3 SBU scanning electron microscope (SEM) with EDS capabilities. The crystals were mounted on carbon tape and analyzed using a 20 kV accelerating voltage and an accumulation time of 20 s. As a qualitative measure, the EDS confirmed the presence of each reported element in the title compounds exclusively.

Optical Spectroscopy. UV−vis diffuse reflectance spectra of polycrystalline powder samples of the reported materials were obtained using a PerkinElmer Lambda 35 UV/vis scanning spectrophotometer equipped with an integrating sphere in the range 200−900 nm. Since many uranyl compounds are luminescent, luminescence spectra of polycrystalline powder samples of the reported materials were obtained using a PerkinElmer LS-55 fluorescence spectrometer. Excitation and emission scans were performed in the 250−450 and 450−900 nm ranges, respectively. The compounds did not exhibit luminescence.

RESULTS AND DISCUSSION

Synthesis. Synthetic uranium silicates have been prepared by solid state reactions,[14] hydrothermal crystal growth,[2−4,6,8−13] and flux crystal growth.[5,7] The majority of the uranium-containing silicates were crystallized using supercritical hydrothermal growth conditions, although a few were grown using mild hydrothermal condition utilizing low temperatures and autogenous pressures. The flux growth method has enjoyed much success for the synthesis of novel complex oxide compositions,[20] and in the case of uranium-containing oxides, halide fluxes have proven to work extremely well.[21−23] To date, only a few uranium silicate materials reported in the literature have been grown as single crystals from the molten flux method. Crystals of $K_6(UO_2)_3Si_8O_{22}$ were grown out of a mixture of KF/KVO_3,[5] while salt-inclusion phases of the form, $\underline{A}[(UO_2)_3(Si_2O_7)_2]$ ($\underline{A}$ = $[K_3Cs_4F]$ and $[NaRb_6F]$), were crystallized from mixed-alkali-metal fluoride fluxes.[7] While targeting the above-mentioned salt-inclusion phases, crystals of "$Cs_2UO_3SiO_3$" and the Rb analog were reported as side products in the reactions of UO_3 and SiO_2 in reactive KF/CsF and NaF/RbF fluxes, respectively, at 750 °C. These compounds are reported to have the same compositions as the title compounds. Only for the cesium phase were lattice parameters provided (they differ from our cesium phase by ∼0.2 Å); however, no further elaboration of these compounds was provided. Deliberate synthesis of phase-pure, high-quality single crystals of the title compounds, Figure 1, was achieved by employing a monocation fluoride flux that also acted as a reagent and a higher reaction temperature, 900 °C.

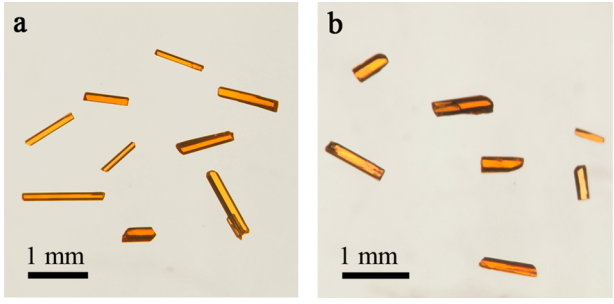

Figure 1. Optical images of Cs_2USiO_6 (a) and Rb_2USiO_6 (b) crystals.

Structures. Cs_2USiO_6 crystallizes in the orthorhombic space group, *Immm*. The structure is composed of UO_6 tetragonal bipyramids, SiO_4 tetrahedra, and Cs^+ ions. The U−O and Si−O bond lengths for the title compounds are listed in Table 2. The uranium atoms are strongly bonded to two oxygen atoms in a linear fashion and exhibit four longer equatorial U−O bonds, consistent with the uranyl bonding motif. The UO_6 octahedra are connected via trans-equatorial oxygen atoms and form infinite chains along the *a* direction, Figure 2. The SiO_4 tetrahedra share corners to form four-membered Si_4O_{12} rings that are located in the *ac* plane. Each UO_6 polyhedron is corner shared to two different Si_4O_{12} rings and to two other UO_6 polyhedra via the remaining two equatorial oxygen atoms, leaving axial terminal uranyl oxygen atoms (Figure 2d), which do not display cation−cation interactions (Type **0**, using the convention published by Read et al.[23]). Each Si_4O_{12} ring structure shares 4 "interior" oxygen atoms between the four SiO_4 tetrahedra (Figure 2d) and the remaining 8 "exterior" oxygen atoms with 8 different UO_6 octahedra, thereby connecting four uranyl based chains. This results in the formation of a true 3D framework that exhibits channels consisting of 10-polyhedra rings (U−Si−U−Si−Si−U−Si−U−Si−Si) along *a*, Figure 3. Cesium cations reside in

Table 2. Selected Interatomic Distances (Angstroms) for Cs_2USiO_6 and the Analogous Average Structure of Rb_2USiO_6

Cs_2USiO_6			Rb_2USiO_6		
U1	O1 × 2	1.861(4)	U1	O1 × 2	1.841(8)
	O2 × 2	2.266(3)		O2A × 2	2.291(11)
	O3 × 2	2.1463(2)		O2B × 2	2.270(11)
Si1	O2 × 2	1.600(3)	Si1	O2A × 2	1.617(11)
	O4	1.6265(16)		O2B × 2	1.541(11)
	O5	1.633(2)		O4	1.627(2)
				O5A × 2	1.610(19)
				O5B × 2	1.64(2)

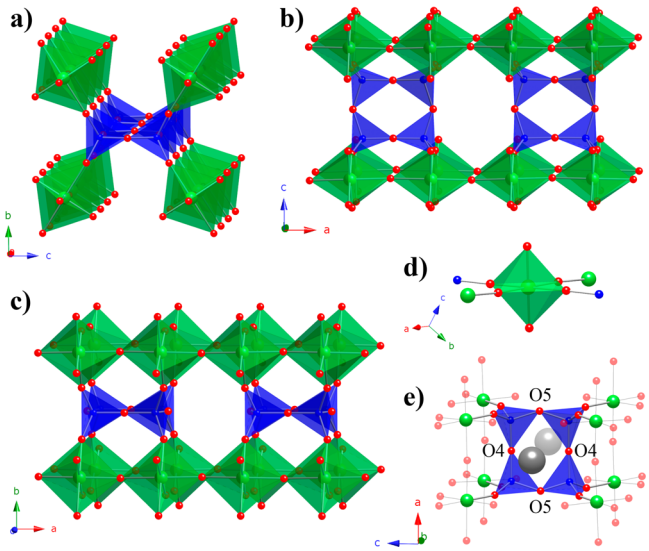

Figure 2. Framework components of Cs_2USiO_6 viewed along the *a* axis (a), *b* axis (b), and *c* axis (c), along with the uranium coordination environment (d) and the Si_4O_{12} tetranuclear rings (e). Cesium, uranium, silicon, and oxygen polyhedra/atoms are shown in gray, green, blue, and red, respectively.

DOI: 10.1021/acs.inorgchem.5b00364
Inorg. Chem. 2015, 54, 4520−4525

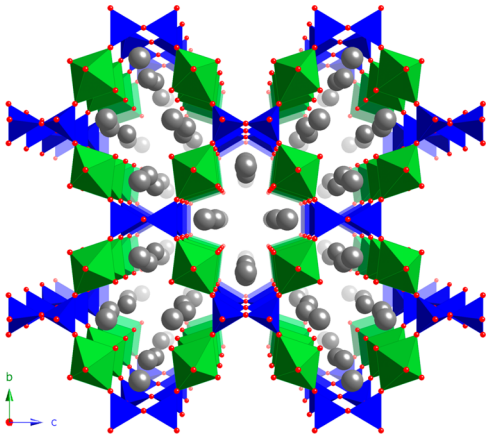

Figure 3. Structure of Cs_2USiO_6 viewed along the *a* axis. Cesium, uranium, silicon, and oxygen polyhedra/atoms are shown in gray, green, blue, and red, respectively. Calculations of the packing indices of the two structures using PLATON were performed using idealized (averaged, nondisordered oxygen atom positions) for the Rb structure. The calculation gave 92.8% filled space for Rb and 95.4% for Cs. The larger volume of free space in the idealized Rb structure correlates with the modulation of the SiO_4 tetrahedra in the true disordered Rb structure, which rotates to fill the free space.

these channels of the framework and are coordinated to 10−12 oxygen atoms at distances of 3.083(3)−3.595(5) Å. A structurally related uranium silicate, $Rb_2(UO_2)(Si_2O_6)\cdot(H_2O)$,[13] has a very similar framework topology, with Rb^+ ions and H_2O molecules residing inside channels made up of similar 10-membered rings. The structural motif based on infinite chains of UO_6 polyhedra and Si_4O_{12} tetranuclear rings has also been observed in $K(UO)Si_2O_6$[4] and $Cs_2K(UO)_2Si_4O_{12}$;[6] however, the reduced uranium-containing UO_6 corner share with four Si_4O_{12} units in the equatorial plane, producing structures with channels of condensed 5-membered rings and 4- and 6-membered rings, respectively.

The rubidium analog, Rb_2USiO_6, shows some added structural complexity, as Rb is too small to coordinate effectively in the isotypic structure with the same periodicity. Using single-crystal X-ray diffraction data, the compound was modeled as being isostructural with Cs_2USiO_6. Two oxygen atoms, O2 and O5, were placed on split positions (see Figure 4), generating a satisfactory refinement with $R_1 = 3.69\%$ for $I > 2\sigma(I)$. The prolate anisotropic displacement of O2 and O5 suggests that there is a slight twisting of the SiO_4 tetrahedra,

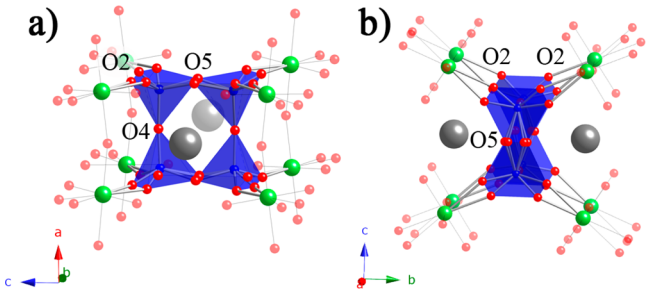

Figure 4. Si_4O_{12} tetranuclear rings in Rb_2USiO_6 modeled in the average *Immm* structure, viewed along the *b* axis (a) and *a* axis (b), showing the modeled split positions of O2 and O5. Rubidium, uranium, silicon, and oxygen polyhedra/atoms are shown in gray, green, blue, and red, respectively.

caused by the need to satisfy the smaller coordination sphere of Rb. This twisting forces the formation of a superstructure with an approximate 6-fold lengthening of the *c* parameter.

Figure 5 shows (a) [100], (b) ⟨−110⟩, (c) [010], and (d) [001] zone axis electron diffraction patterns (EDPs) of Rb_2USiO_6. In addition to the set of generally strong Bragg reflections (labeled **G** hereafter) of an underlying *P*-centered (but close to *Immm*) average structure, one observes the clear presence of additional incommensurate satellite reflections at $\mathbf{G} \pm m\mathbf{q}$, where *m* is an integer and the incommensurate primary modulation wave vector $\mathbf{q} = 0.839(5)\mathbf{c}^*$, i.e., very close to 5/6. The 4-integer *hklm* indexation in Figure 5 is thus with respect to the four basis vectors $\mathbf{a}^*$, $\mathbf{b}^*$, $\mathbf{c}^*$, and $\mathbf{q}$. Note that the incommensurate satellite reflections drop off systematically in intensity with increasing harmonic order and can be observed (but only just) up to order $m = 3$.

Given that the average structure of Rb_2USiO_6, i.e., the structure obtained by ignoring the latter satellite reflections, was successfully refined in space group *Immm* (with split O2 and O5 oxygen atom positions), it was expected that the observed *hklm* reflections would exhibit the superspace centering condition $F(hklm) = 0$ unless $h + k + l$ is even. The observation of quite weak but clearly present reflections such as −1,−1,1,0 and −1,−1,1,−1 (arrowed in blue in Figure 5b) or −1,0,2,0 (arrowed in blue in Figure 5c), however, are incompatible with $\{x_1 + 1/2, x_2 + 1/2, x_3 + 1/2, x_4\}$ superspace centering. There must therefore have a weak $\mathbf{q} = \mathbf{c}^*$ modulation of the average structure which lowers the space group symmetry from *Immm* to a *P*-centered subgroup thereof. The presence of the condition $F(0KLM) = 0$ unless $K + L$ is even in Figure 5a implies a superspace symmetry operation of $\{-x_1 + 1/2, x_2 + 1/2, x_3 + 1/2, x_4\}$ and an *n* glide of the parent (or average) structure perpendicular to **a**. Likewise, the condition $F(HK00) = 0$ unless $H + K$ is even in Figure 5d implies a superspace symmetry operation of $\{x_1 + 1/2, x_2 + 1/2, -x_3 + 1/2, -x_4 + 2\delta\}$ and, again, an *n* glide of the parent structure perpendicular to **c**. On the other hand, the presence of reflections such as −1,0,2,0 (arrowed in blue) and 101−1 etc. in Figure 5c do not necessitate the existence of a superspace symmetry operation. The likely overall superspace symmetry is thus $Pn2n(00,\gamma \approx 0.839)$, a nonstandard setting of the superspace group $P2nn(00,\gamma \approx 0.839)$, No. 34.4 in Table 9.8.3.5 of Janssen et al.[24]

On the basis of the electron diffraction data, it appears that the average or parent structure is thus a minimum of *Pn2n* (potentially also *Pnmn*) due to the combination of the incommensurate modulation associated with the incommensurate primary modulation wave vector $\mathbf{q} = 0.839(5)\mathbf{c}^*$ coupled with a weak $\mathbf{q} = \mathbf{c}^*$ modulation of the initially refined *Immm* "grandparent" structure.

Refinements of the average structure were carried out in multiple space groups; however, it was found that using the single-crystal diffraction data collected on a high-quality crystal of Rb_2USiO_6 the solution and refinement in the *Immm* subcell gave the best answer. Ultimately, as the overall structure is actually incommensurate, the determination of an average, commensurate structure in *Immm* provides us with the most useful structural representation at this time.

The bond valence sums for each cation have been calculated for the title compounds and are listed in Table 3. For Rb_2USiO_6, BVS values were calculated using an average of the split O2 and O5 positions. The optimized parameters provided by Burns,[25] $r_{U-O} = 2.051$ and $b = 0.519$, were used for

DOI: 10.1021/acs.inorgchem.5b00364
Inorg. Chem. 2015, 54, 4520−4525

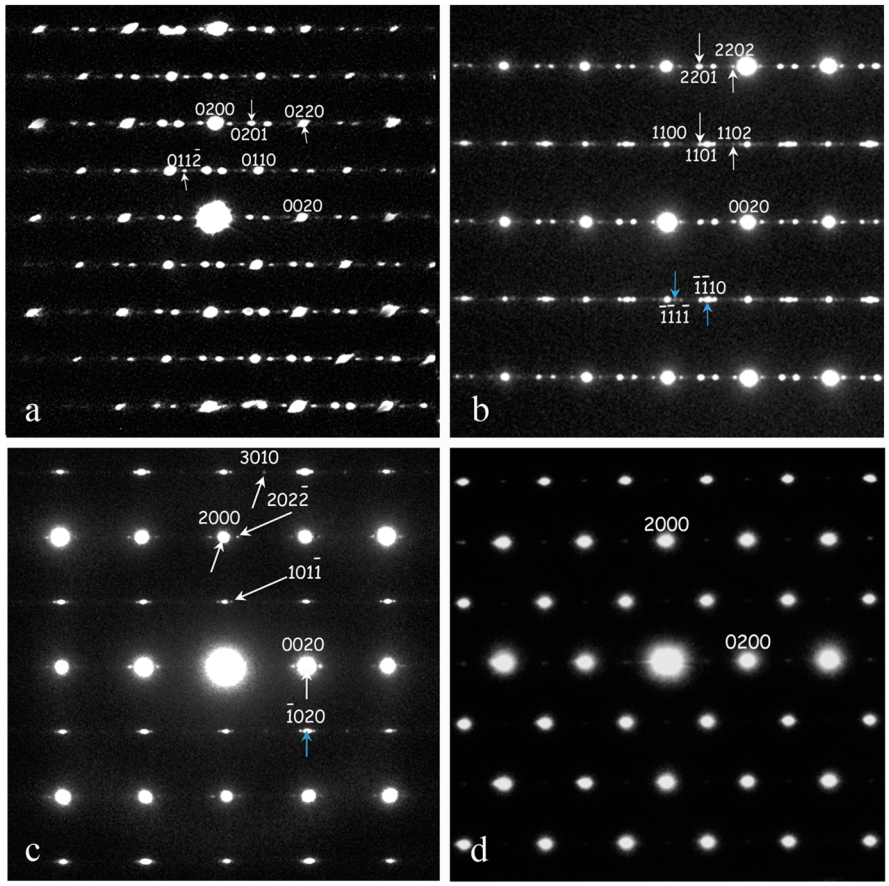

Figure 5. (a) [100], (b) ⟨−110⟩, (c) [010], and (d) [001] zone axis electron diffraction patterns (EDPs) of Rb_2USiO_6.

Table 3. Bond Valence Sums for Cs_2USiO_6 and Rb_2USiO_6, Where an Average of the Split O2 and O5 Positions Modeled in the *Immm* Structure Was Used To Calculate the BVS Values for the Latter

Cs_2USiO_6		Rb_2USiO_6	
U1	5.87	U1	5.98
Si1	4.28	Si1	4.43
Cs1	1.03	Rb1	1.09
Cs2	1.10	Rb2	1.09
Cs3	1.01	Rb3	0.99
Cs4	0.95	Rb4	1.22

calculating the U−O valences. The BVS values of 5.87−5.98 (U), 4.28−4.43 (Si), 0.95−1.10 (Cs), and 0.99−1.22 (Rb) are all in agreement with U^{6+}, Si^{4+}, Cs^{+}, and Rb^{+}. The slightly high values for Si and Rb (>10% difference) can be attributed to the imperfect structure model.

Optical Spectroscopy. UV−vis diffuse reflectance data were measured on ground crystals of the title compounds and converted to absorbance vs wavelength plots using the Kubelka−Munk function.[26] Both compounds displayed a broad absorption band covering 200−550 nm (see Figure S3, Supporting Information). The band gaps of 2.18−2.19 eV, estimated as the *x* intercept of the line tangent to the absorption edge, sugges that these materials can be classified as semiconductors.

CONCLUSIONS

High-quality single crystals of Cs_2USiO_6 and Rb_2USiO_6 were grown from molten fluoride fluxes. The effect of the size of the alkali-metal cation is evident in both single-crystal X-ray diffraction and electron diffraction data. The smaller size of the Rb cation forces an approximate 6-fold superstructure, with a slight lowering of the symmetry from the space group *Immm* (No. 71) to the superspace group *Pn*2*n* (No. 34.4). The semiconducting compounds did not exhibit luminescence at room temperature.

ASSOCIATED CONTENT

Supporting Information

Powder XRD patterns, UV−vis spectra, atomic coordinates and equivalent isotropic displacement parameters, and additional crystallographic comments on the 6-fold superstructure of Rb_2USiO_6. This material is available free of charge via the Internet at http://pubs.acs.org. Further details of the crystal structure investigation can be obtained from the Fachinformationszentrum Karlsruhe, 76344 Eggenstein-Leopoldshafen, Germany (fax +497247808666; e-mail crystdata@fiz-karlsruhe.de) on quoting depository numbers CSD-429209 and CSD-429210.

AUTHOR INFORMATION

Corresponding Author

*Phone: (803) 777-6916. Fax: (803) 777-8508. E-mail: zurloye@mailbox.sc.edu.

DOI: 10.1021/acs.inorgchem.5b00364
Inorg. Chem. 2015, 54, 4520−4525

Notes

The authors declare no competing financial interest.

■ ACKNOWLEDGMENTS

Research was supported by the U.S. Department of Energy, Office of Basic Energy Sciences, Division of Materials Sciences and Engineering under Award DE-SC0008664. Electron diffraction measurements were carried out at the Australian National University.

■ REFERENCES

(1) Ojovan, M. I.; Lee, W. E. *An Introduction to Nuclear Waste Immobilization*, 2nd ed.; Elsevier: Amsterdam, 2014.
(2) Chen, C.-S.; Kao, H.-M.; Lii, K.-H. *Inorg. Chem.* **2005**, *44*, 935−940.
(3) Chen, C. L.; Nguyen, Q. B.; Chen, C. S.; Lii, K. H. *Inorg. Chem.* **2012**, *51*, 7463−7465.
(4) Chen, C. S.; Lee, S. F.; Lii, K. H. *J. Am. Chem. Soc.* **2005**, *127*, 12208−12209.
(5) Lee, C.-S.; Wang, S.-L.; Lii, K. H. *Chem. J. Chi. Univ.* **2011**, *32*, 605−608.
(6) Lee, C. S.; Wang, S. L.; Lii, K. H. *J. Am. Chem. Soc.* **2009**, *131*, 15116−15117.
(7) Lee, C. S.; Wang, S. L.; Chen, Y. H.; Lii, K. H. *Inorg. Chem.* **2009**, *48*, 8357−8361.
(8) Lee, C. S.; Lin, C. H.; Wang, S. L.; Lii, K. H. *Angew. Chem., Int. Ed. Engl.* **2010**, *49*, 4254−4256.
(9) Lin, C. H.; Chen, C. S.; Shiryaev, A. A.; Zubavichus, Y. V.; Lii, K. H. *Inorg. Chem.* **2008**, *47*, 4445−4447.
(10) Liu, H. K.; Lii, K. H. *Inorg. Chem.* **2011**, *50*, 5870−5872.
(11) Liu, H. K.; Chang, W. J.; Lii, K. H. *Inorg. Chem.* **2011**, *50*, 11773−11776.
(12) Pointeau, V.; Deditius, A. P.; Miserque, F.; Renock, D.; Becker, U.; Zhang, J.; Clavier, N.; Dacheux, N.; Poinssot, C.; Ewing, R. C. *J. Nucl. Mater.* **2009**, *393*, 449−458.
(13) Huang, J.; Wang, X.; Jacobson, A. J. *J. Mater. Chem.* **2003**, *13*, 191−196.
(14) Plaisier, J. R.; Ijdo, D. J. W.; de Mello Donega, C.; Blasse, G. *Chem. Mater.* **1995**, *7*, 738−743.
(15) Rosenweig, A.; Ryan, R. R. *Am. Mineral.* **1975**, *60*, 448−453.
(16) Stohl, F. V.; Smith, D. K. *Am. Mineral.* **1981**, *66*, 610−625.
(17) *SMART Version 5.630, SAINT+ Version 6.45, and SADABS Version 2.10*; Bruker Analytical X-ray Systems, Inc.: Madison, WI, 2003.
(18) Sheldrick, G. M. *Acta Crystallogr. A* **2008**, *64*, 112−122.
(19) ShelXle: a Qt graphical user interface for SHELXL: Hübschle, C. B.; Sheldrick, G. M.; Bittrich, B. *J. Appl. Crystallogr.* **2011**, *44*, 1281−1284.
(20) Bugaris, D. E.; zur Loye, H.-C. *Angew. Chem., Int. Ed. Engl.* **2012**, *51*, 3780−3811.
(21) Read, C. M.; Smith, M. D.; zur Loye, H.-C. *J. Chem. Crystallogr.*, submitted.
(22) Read, C. M.; Smith, M. D.; zur Loye, H.-C. *Solid State Sci.* **2014**, *37*, 136−143.
(23) Read, C. M.; Yeon, J.; Smith, M. D.; zur Loye, H.-C. *Cryst. Eng. Commun.* **2014**, *16*, 7259−7267.
(24) Janssen, T.; Janner, A.; Looijenga-Vos, A.; de Wolff, P. M. Incommensurate and Commensurate Modulated Structures. In *International Tables for Crystallography*; Wilson, A. J. C., Ed.; Kluwer Academic Publishers: Dordrecht, 1995; Vol. *C*, pp 797−844.
(25) Burns, P. C.; Ewing, R. C.; Hawthorne, F. C. *Can. Mineral.* **1997**, *35*, 1551−1570.
(26) Kubelka, P.; Munk, F. Z. *Technol. Phys.* **1931**, *12*, 593−601.

DOI: 10.1021/acs.inorgchem.5b00364
Inorg. Chem. 2015, 54, 4520−4525